

Spectral properties near the Mott transition in the two-dimensional t - J model

Masanori Kohno

WPI Center for Materials Nanoarchitectonics, National Institute for Materials Science, Tsukuba 305-0044, Japan

(Dated: August 29, 2018)

The single-particle spectral properties of the two-dimensional t - J model in the parameter regime relevant to cuprate high-temperature superconductors are investigated using cluster perturbation theory. Various anomalous features observed in cuprate high-temperature superconductors are collectively explained in terms of the dominant modes near the Mott transition in this model. Although the behavior of the dominant modes in the low-energy regime is similar to that in the two-dimensional Hubbard model, significant differences appear near the Mott transition for the high-energy electron removal excitations which can be considered to primarily originate from holon modes in one dimension. The overall spectral features are confirmed to remain almost unchanged as the cluster size is increased from 4×4 to 6×6 sites by using a combined method of the non-abelian dynamical density-matrix renormalization group method and cluster perturbation theory.

PACS numbers: 71.30.+h, 71.10.Fd, 74.72.Kf, 79.60.-i

I. INTRODUCTION

Cuprate high-temperature (high- T_c) superconductors, which are obtained by doping Mott insulators containing CuO_2 planes,¹ exhibit various features that appear anomalous from conventional viewpoints.²⁻¹³ Because the anomalous features are considered to be related to high- T_c superconductivity, the effects of electronic correlations near the Mott transition in two-dimensional (2D) systems have attracted considerable attention.¹²⁻¹⁷ In particular, through an analysis of electronic correlations among relevant Cu and O orbitals, the 2D t - J model has been derived as a minimal model of high- T_c cuprates.¹⁸ However, its properties and their relationship to the anomalous features are not well understood, primarily because of difficulties in dealing with the no-double-occupancy constraint.

Although this model can also be derived effectively from the 2D Hubbard model in the large-repulsion limit,¹⁹ it is not clear how similar the two models' properties are in the parameter regime relevant to high- T_c cuprates. In fact, the 2D t - J and Hubbard models have frequently been studied from different viewpoints: the former has been considered a doped Mott insulator accessible from slave-particle theories,^{15,16} while the latter has been considered a strongly interacting electron system accessible from Fermi liquid theory.¹⁷ In some studies, double occupancy, which is excluded in the t - J model, has been considered important to the anomalous features.²⁰⁻²⁴

In this paper, by using cluster perturbation theory (CPT),^{25,26} similarities and dissimilarities in the spectral features of these models are clarified. In addition, various anomalous features observed in high- T_c cuprates are collectively explained in the 2D t - J model, which is an effective model of the CuO_2 plane and has no double occupancy. A method to reduce cluster-size effects is also introduced.

II. MODELS AND METHODS

A. Models

We consider the 2D t - J model defined by the following Hamiltonian for $t > 0$ and $J > 0$:

$$\mathcal{H} = -t \sum_{\langle i,j \rangle \sigma} (\tilde{c}_{i\sigma}^\dagger \tilde{c}_{j\sigma} + \text{H.c.}) + J \sum_{\langle i,j \rangle} (\mathbf{S}_i \cdot \mathbf{S}_j - \frac{1}{4} n_i n_j) - \mu \sum_i n_i,$$

where $\tilde{c}_{i\sigma} = (1 - n_{i,-\sigma})c_{i\sigma}$ and $n_i = \sum_\sigma n_{i\sigma}$ for the annihilation operator $c_{i\sigma}$ and number operator $n_{i\sigma}$ of an electron with spin σ at site i . Here, \mathbf{S}_i denotes the spin operator at site i , and $\langle i,j \rangle$ means that sites i and j are nearest neighbors on a square lattice. At half-filling (doping concentration $\delta = 0$), the model reduces to the Heisenberg model. The t - J model can also be effectively obtained for $J = 4t^2/U$, by neglecting the three-site term,^{16,19} in the large- U/t limit of the Hubbard model defined by the following Hamiltonian:

$$\mathcal{H}_{\text{Hub}} = -t \sum_{\langle i,j \rangle \sigma} (c_{i\sigma}^\dagger c_{j\sigma} + \text{H.c.}) + U \sum_i n_{i\uparrow} n_{i\downarrow} - \mu \sum_i n_i.$$

In the ground state near the Mott transition, ferromagnetic fluctuations might be dominant in the very small- J/t regime,²⁷⁻²⁹ and phase separation occurs in the large- J/t regime.^{13,16,30-38} Here, focusing attention on the parameter regime relevant to high- T_c cuprates ($J/t \approx 0.5$),^{13,16} where the CPT results exhibit no indication of phase separation [Fig. 1(m)], we study the spectral function defined as $A(\mathbf{k}, \omega) = -\text{Im}G(\mathbf{k}, \omega)/\pi$. Here, $G(\mathbf{k}, \omega)$ denotes the retarded single-particle Green function for momentum \mathbf{k} and frequency ω at zero temperature.^{12,13}

B. Methods

In this paper, CPT is employed: $G(\mathbf{k}, \omega)$ is calculated by connecting cluster Green functions

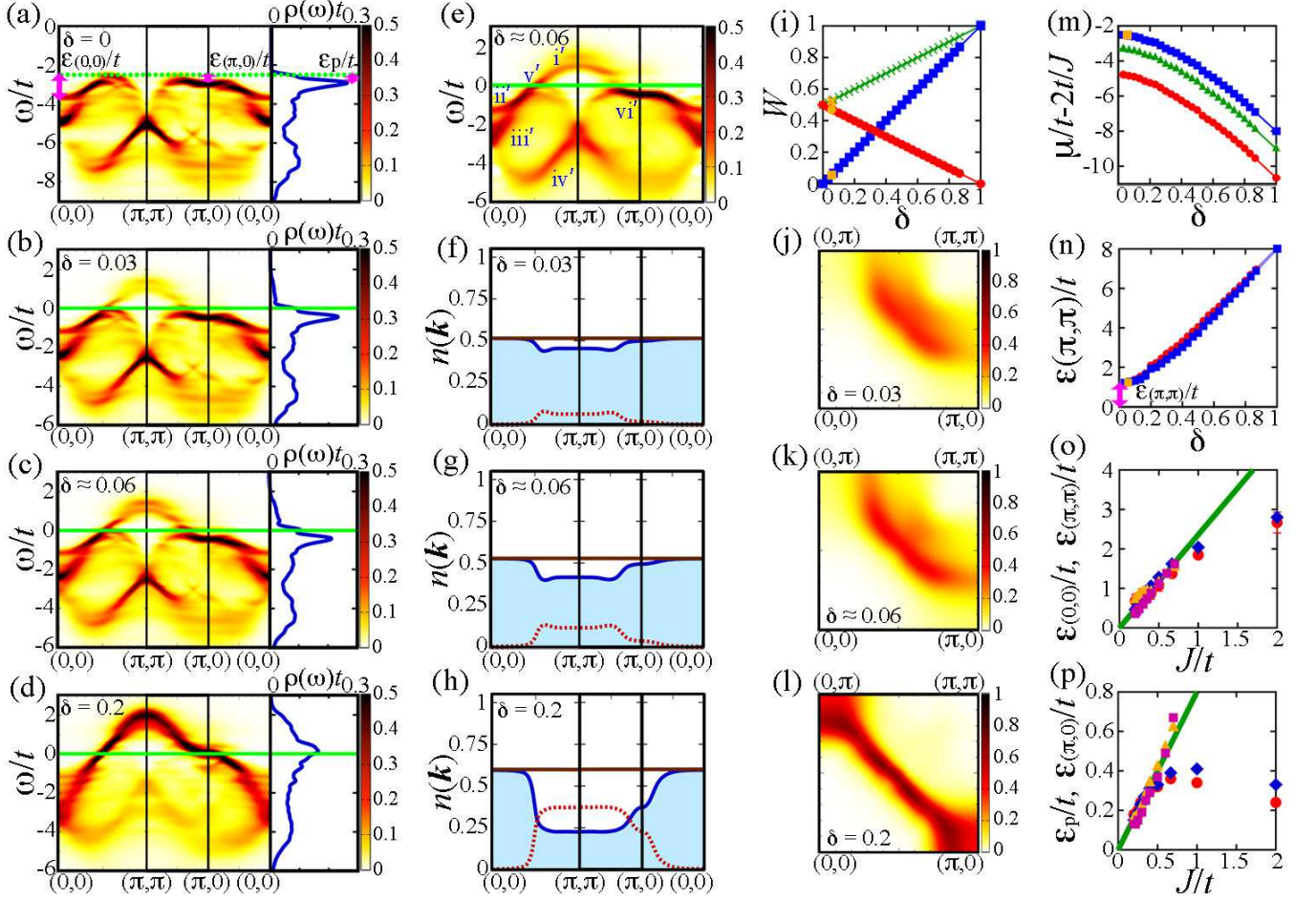


FIG. 1: Results for the 2D t - J model obtained using (4×4) -site CPT [(a)–(d) and (f)–(p)] and (6×6) -site CPT [(e); yellow symbols in (i), (m), and (n) for $J/t = 0.5$ at $\delta = 1/18$]. (a)–(d) $A(\mathbf{k}, \omega)t$ for $J/t = 0.5$ at $\delta = 0$ ($\mu/t = 4$), 0.03, $1/18$ (≈ 0.06), and 0.2 (from above). The rightmost panels show $\rho(\omega)t \equiv \int d\mathbf{k} A(\mathbf{k}, \omega)t / (2\pi)^d$ in $d(=2)$ dimensions. The dotted green line in (a) indicates ω at the top of the band. The solid green lines in (b)–(d) indicate $\omega = 0$. (e) The same as the left panels of (c) but using (6×6) -site CPT. The blue numbers indicate dominant modes. (f)–(h) $n(\mathbf{k}) [\equiv \int_{\omega_{\text{range}}} d\omega A(\mathbf{k}, \omega)]$ for (b)–(d) for $\omega < 0$ [$n_-(\mathbf{k})$] (solid blue curves with hatches), $\omega > 0$ (dotted red curves), and all ω [$n_t(\mathbf{k})$] (solid brown lines). (i) Spectral weight $W [\equiv \int_{\omega_{\text{range}}} d\omega \rho(\omega)]$ for $\omega < 0$ [W_-] (red circles), $\omega > 0$ [W_+] (blue squares), and all ω (green crosses) at $J/t = 0.5$. (j)–(l) The same as in (b)–(d) but for $\omega \approx 0$. (m) Chemical potential μ for $J/t = 0.5, 0.4$, and 0.3 (from above). (n) Energy of mode i' at (π, π) [$\varepsilon(\pi, \pi)$] (blue squares) for $J/t = 0.5$. (o) $\varepsilon_{(0,0)}$ (purple squares) and $\varepsilon_{(\pi,\pi)}$ (yellow triangles). The solid green line indicates $\sqrt{2}v_s/t$ ($v_s \approx 1.18\sqrt{2}$ [39]). (p) ε_p (purple squares) and $\varepsilon_{(\pi,0)}$ (yellow triangles). The solid green line is proportional to J . The red circles in (n) and blue diamonds and red circles in (o) and (p) indicate corresponding energies in the 2D Hubbard model ($U/t = 4t/J$), taken from Ref. 40. Gaussian broadening with a standard deviation of $0.1t$ is used.

through the first-order hopping process.^{25,26,40–43} By considering superclusters, $G(\mathbf{k}, \omega)$ at arbitrary δ can be obtained.²⁶ In the large-cluster limit, CPT becomes exact. Here, to calculate the (4×4) -site and (6×6) -site cluster Green functions, exact diagonalization and the dynamical density-matrix renormalization group (DDMRG) method⁴⁴ are used, respectively. In the DDMRG calculation, the $U(1) \otimes SU(2)$ basis^{45,46} is employed,⁴⁷ and 1000 density-matrix eigenstates are retained.

The DDMRG method and CPT work well together because of the following reasons. (1) It is not necessary to repeat DDMRG calculations because CPT does not

impose self-consistency. (2) Data under open boundary conditions, which are obtained accurately in the DDMRG method, are used in CPT. The combined method can be regarded either as CPT where the DDMRG method is utilized as a cluster Green function solver or as the DDMRG method where momenta are interpolated based on CPT. Note that real-space cluster Green functions are used in the combined method [Fig. 1(e)] in contrast with the random-phase approximation (RPA) from the decoupled-chain limit⁴⁸ using DDMRG results [Figs. 2(c) and 2(f)].⁴⁰ In this paper, the RPA from the decoupled-chain limit, which corresponds to the perturbation theory up to the first order with respect to interchain hopping, is

only used to explain how the spectral weights are shifted by interchain hopping from the decoupled-chain limit and to trace the origins of the dominant modes of 2D systems back to those of one-dimensional (1D) systems (Secs. III A and III D).

C. Cluster-size effects

As shown in Figs. 1(c), 1(e), 1(i), 1(m), and 1(n), the results obtained using (6×6) -site CPT are almost the same as those using (4×4) -site CPT. This implies that the overall spectral features will not change significantly if the cluster size is increased.

III. SPECTRAL PROPERTIES

A. Dominant modes

The results for the 2D t - J model obtained using CPT are shown in Fig. 1. The overall spectral features can be explained in terms of the dominant modes [Fig. 1(e), modes i' - vi'] corresponding to those of the 2D Hubbard model [Fig. 2(g), modes i - vi],⁴⁰ whose origins can be traced back to those of the 1D models [Fig. 2(d), modes $1'$ - $5'$; Fig. 2(a), modes 1 - 5]⁴⁹⁻⁵⁷ by considering how the spectral weights are shifted by interchain hopping from the decoupled-chain limit [Figs. 2(c) and 2(f); Sec. III D].^{40,42,58,59} The dispersing mode around (π, π) for $\omega > 0$, mode i' (\approx mode i), originates from mode $1'$ (\approx mode 1, upper edge of the spinon-antiholon continuum). The mode around $(0, 0)$ for $\omega \lesssim 0$, mode ii' (\approx mode ii), primarily originates from mode $2'$ (\approx mode 2, spinon mode), and the mode for slightly lower ω , mode iii' (\approx mode iii), primarily originates from mode $3'$ (\approx mode 3, holon mode). The mode spreading over the Brillouin zone in the large negative ω regime, mode iv' (\approx mode iv), primarily originates from mode $4'$ (\approx mode 4, holon mode called the shadow band). The mode bending back around $(\pi/2, \pi/2)$ for $\omega \gtrsim 0$ (\approx upper edge of the band around $(\pi/2, \pi/2)$ at half-filling), mode v' (\approx mode v), originates from mode $5'$ (\approx mode 5, antiholon mode). The flat mode, mode vi' (\approx mode vi), is dominant around $(\pi, 0)$.

B. Positive ω

Mode i' corresponds to the doping-induced states observed in high- T_c cuprates and in theoretical calculations^{3,4,12,13,20-24,32,40,42,60-76} with controversial interpretations. The CPT results indicate that the energy of this mode at (π, π) [$\varepsilon(\pi, \pi)$] does not reach zero even in the small-doping limit [Fig. 1(n)]. The extrapolated value of $\varepsilon(\pi, \pi)$ to $\delta \rightarrow 0$ [$\varepsilon(\pi, \pi)$] behaves essentially as $\sqrt{2}v_s$ in the small- J/t regime, where v_s

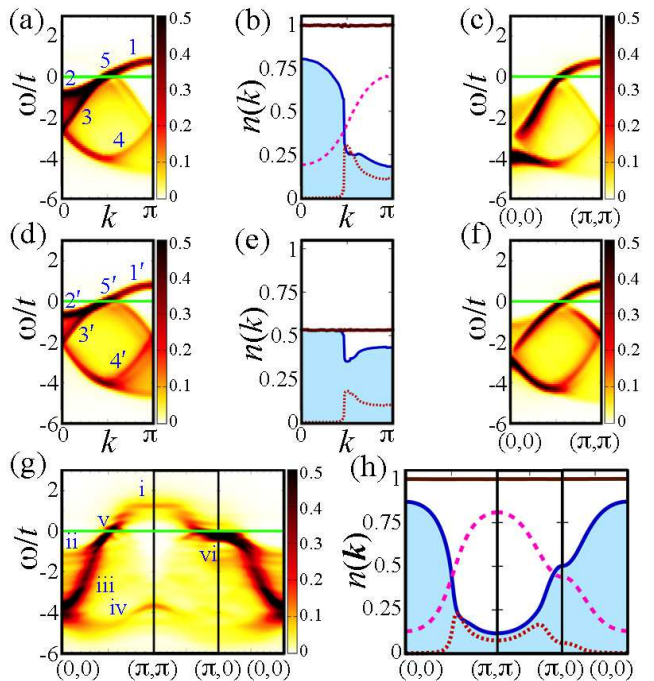


FIG. 2: (a) $A(k, \omega)t$ for $U/t = 8$ at $\delta = 1/15 (\approx 0.07)$ for the lower Hubbard band (LHB) of the 1D Hubbard model⁴⁹ on a 120-site chain obtained using the non-abelian DDMRG method with 120 density-matrix eigenstates. The blue numbers indicate dominant modes. (b) $n(k)$ for (a) for $\omega < 0$ [$n_-(k)$] (solid blue curve with hatches), $\omega > 0$ in the LHB (dotted red curve), the upper Hubbard band (dashed pink curve), and all ω [$n_t(k)$] (solid brown line).⁴⁹ (c) RPA results for $t_\perp = t$ obtained using the data in (a).⁴⁰ (d)-(f) The same as (a)-(c) but for the t - J model at $J/t = 0.5$. (g) The same as the left panels of Fig. 1(c) but for the LHB of the 2D Hubbard model at $U/t = 8$.⁴⁰ The blue numbers indicate dominant modes. (h) $n(k)$ for (g) with the same line types as in (b).⁴⁰ The solid green lines indicate $\omega = 0$. Gaussian broadening with a standard deviation of $0.1t$ is used.

denotes the spin-wave velocity of the 2D Heisenberg model ($v_s \approx 1.18\sqrt{2}J$ [39]) [Fig. 1(o)], as in the 2D Hubbard model.⁴⁰ In addition, the spectral weight for $\omega > 0$ (W_+) behaves exactly as δ [Fig. 1(i)].^{32,75} These results imply that mode i' continuously leads to the magnetic excitation of the Mott insulator, while its spectral weight gradually disappears toward the Mott transition. This feature is essentially the same as that in the 1D and 2D Hubbard models^{40,49,62} and is consistent with a general argument in the small-doping limit.⁴⁷ Thus, this feature will be related to transformation to the Mott insulator, which has low-energy spin excitation but no low-energy charge excitation (spin-charge separation), rather than being related to double occupancy.

Because mode v' bends back around $(\pi/2, \pi/2)$ for $\omega \gtrsim 0$ [Figs. 1(b), 1(c), and 1(e)], there are small intensities at momenta slightly away from $(\pi/2, \pi/2)$ toward (π, π) as well as significant intensities around $(\pi/2, \pi/2)$ for $\omega \approx 0$ near the Mott transition [Figs. 1(j) and 1(k)].⁴⁰

The region surrounded by these intensities might be effectively regarded as a hole pocket. Regarding hole pockets, the momentum distribution function $n_-(\mathbf{k})$ has been investigated,^{13,75–83} a high momentum resolution is desired near the Mott transition at zero temperature. The CPT results indicate that $n_-(\mathbf{k})$ exhibits a small dip near $(\pi/2, \pi/2)$ [Figs. 1(f) and 1(g)], for which mode v' would be more or less responsible.^{47,69,76}

C. Small negative ω

The bandwidth of mode ii' at half-filling [$\varepsilon_{(0,0)}$] [Fig. 1(a)] has been studied in relation to the hole motion in an antiferromagnet, and its J dependence (particularly the power-law behavior in the small- J/t regime) has been discussed.^{13,43,66,68,84–98} Figure 1(o) indicates that it behaves essentially as $\sqrt{2}v_s$ in the small- J/t regime, as in the 2D Hubbard model.^{40,42,62} The bifurcation between this mode and mode iii' as well as the reduction in spectral weight just below the bifurcation point [Figs. 1(b), 1(c), and 1(e)] can be identified⁴⁰ as the giant kink and waterfall behavior observed in high- T_c cuprates^{7–11} for which various interpretations have been proposed.^{7–11,20,21,40,72,73,99–101} Modes ii' and iii' correspond to spinon-like and holon-like branches observed in high- T_c cuprates,⁷ respectively.

The properties around $(\pi, 0)$ are primarily characterized by mode vi' , which corresponds to the flat band observed in high- T_c cuprates and in theoretical calculations.^{5,12,13,40,63–66,71,73,93–97,102} Because this mode carries large spectral weights and exhibits an almost flat dispersion relation over a wide momentum range around $(\pi, 0)$, it significantly contributes to the main peak of the single-particle density of states $\rho(\omega)$ [Figs. 1(a)–1(c)]. For instance, as shown in Fig. 1(p), the energy difference of the main peak of $\rho(\omega)$ from the top of the band at half-filling [ε_p] [Fig. 1(a)] is primarily determined by that of this mode at $(\pi, 0)$ [$\varepsilon_{(\pi,0)}$] [Fig. 1(a)]. This energy difference, which can be regarded as a pseudogap in the small-doping limit, will be related to the antiferromagnetic fluctuation because it is almost proportional to J in the small- J/t regime [Fig. 1(p)], as in the 2D Hubbard model.^{40,63,65}

Near the Mott transition, because mode vi' is located below $\omega = 0$, there is no mode crossing $\omega = 0$ along $(0, 0)$ – $(\pi, 0)$, and the spectral weights along $(\pi, 0)$ – (π, π) for $\omega \approx 0$ are also reduced significantly [Figs. 1(b), 1(c), 1(e), 1(j), and 1(k)].⁴⁰ Thus, the spectral weights for $\omega \approx 0$ essentially remain only around $(\pi/2, \pi/2)$, which corresponds to the Fermi arc behavior observed in high- T_c cuprates.^{2,6}

In the large-doping regime, the behavior becomes similar to that of non-interacting electrons after the pseudogap closes [the peak of $\rho(\omega)$ or the flat mode crosses $\omega = 0$] [Figs. 1(d), 1(h), and 1(l)].^{40,63–66}

D. Large negative ω

Although mode iv' corresponds to mode iv , its spectral weights around $(0, 0)$ and (π, π) are significantly smaller and larger, respectively, and its ω values around $(0, 0)$ and (π, π) are significantly higher than those of mode iv near the Mott transition [Figs. 1(b), 1(c), 1(e), and 2(g)]. Similar features have also been obtained primarily at half-filling using exact diagonalization¹⁰³ and recently using CPT independently.⁴³ Here, we interpret these features as a consequence of the restriction on spectral weights.

For the electron operators with the no-double-occupancy constraint, $\hat{c}_{i\sigma}^{(\dagger)}$, the spectral weight for each \mathbf{k} [$n_t(\mathbf{k})$] is reduced to $(1 + \delta)/2$ [75] [Figs. 1(f)–1(h) and 2(e)]. As a result, the spectral weight for $\omega < 0$ [$n_-(\mathbf{k})$] around $\mathbf{k} = \mathbf{0}$ in the t - J model becomes significantly smaller than that of the Hubbard model near the Mott transition [Figs. 1(g) and 2(h); Figs. 2(e) and 2(b)]. Because the spectral weight for $\omega < 0$ (W_-) is equal to $(1 - \delta)/2$ in the t - J and Hubbard models, $n_-(\mathbf{k})$ around $\mathbf{k} = \boldsymbol{\pi}$ in the t - J model becomes larger to compensate for the reduction around $\mathbf{k} = \mathbf{0}$. Here, $\mathbf{0}$ and $\boldsymbol{\pi}$ indicate 0 and π for 1D systems and $(0, 0)$ and (π, π) for 2D systems, respectively.

In the RPA from the decoupled-chain limit [$G^{-1}(\mathbf{k}, \omega) = G_{1D}^{-1}(k_x, \omega) - t_{\perp}(\mathbf{k})$],⁴⁸ the spectral weights shift upward and downward in the momentum regime for $t_{\perp}(\mathbf{k}) > 0$ and $t_{\perp}(\mathbf{k}) < 0$, respectively,^{40,42,58,59} where $G_{1D}(k_x, \omega)$ and $t_{\perp}(\mathbf{k}) (= -2t_{\perp} \cos k_y)$ denote the Green function of a chain and Fourier transform of the interchain hopping integral, respectively. In addition, the mode shift becomes large if the mode carries large spectral weights in the large- $|t_{\perp}(\mathbf{k})|$ regime.^{40,42,58,59} Because the spectral weight around $k = 0$ for $\omega < 0$ in the 1D t - J model is significantly smaller, the downward spectral-weight shift around $(0, 0)$ is smaller [Fig. 2(f)] than that of the Hubbard model [Fig. 2(c)].

This argument explains why the ω value around $(0, 0)$ of mode iv' is higher than that of mode iv near the Mott transition [Figs. 1(c) and 2(g)]. For (π, π) , a similar argument can also explain that the ω value around (π, π) of mode iv' is higher than that of mode iv . Near the Mott transition, however, the ω values of modes 4, 4', iv , and iv' around $\mathbf{k} = \boldsymbol{\pi}$ appear to be better explained by considering that they are almost the same as those around $\mathbf{k} = \mathbf{0}$ [Figs. 1(a)–1(c), 1(e), 2(a), 2(d), and 2(g)]. At half-filling, the ω value of mode 4 at $k = \pi$ is exactly the same as that at $k = 0$ because the dispersion relation of the holon mode becomes symmetric with respect to $k = \pi/2$.^{49,51,104}

For the differences in the large negative ω regime, the neglect of the three-site term is relevant,^{43,103} because this term contributes to hopping.

IV. DISCUSSION AND SUMMARY

In this study, the single-particle spectral properties of the 2D t - J model for $J/t \approx 0.5$ near the Mott transition were investigated. In contrast with conventional exact diagonalization studies, where the spectral weights were calculated only at available \mathbf{k} and δ points depending on the cluster size and boundary conditions, the spectral-weight distributions for continuous \mathbf{k} and ω near the Mott transition with small intervals of δ were calculated using CPT, and how the peaks of the spectral weights form dominant modes and how the modes transform to those of the Mott insulator as δ gradually decreases were clarified in the 2D t - J model. In addition, through comparisons of the (4×4) -site CPT results with the (6×6) -site CPT results obtained by combining the non-abelian DDMRG method, the cluster-size effects were confirmed to be small enough to allow discussion on the overall spectral features.

Furthermore, the natures of the dominant modes in the 2D t - J model were clarified by investigating the δ and J/t dependences of the characteristic energies and spectral weights and by tracing the origins of the modes back to those of the 1D models. In terms of the dominant modes, various anomalous spectral features observed in high- T_c cuprates, such as the doping-induced states, flat band, pseudogap, Fermi arc, spinon-like and holon-like branches, giant kink, and waterfall behavior,²⁻¹³ were collectively explained in the 2D t - J model, as in the 2D Hubbard model.⁴⁰

The results for the natures of the dominant modes imply that these spectral features are primarily related

to the proximity of the antiferromagnetic Mott insulator, which has a low-energy spin-wave mode¹⁰⁵ but no low-energy charge excitation, and to the existence of different energy scales that characterize the bandwidths of the dominant modes rather than to double occupancy, which is completely removed in the 2D t - J model.

Although the spectral features of the 2D t - J model in the small- $|\omega|$ regime are similar to those of the 2D Hubbard model, significant differences appear in the large negative ω regime around $(0, 0)$ and (π, π) near the Mott transition for the modes which can be considered to primarily originate from the 1D holon modes. In this study, the differences were interpreted as a consequence of the restriction on spectral weights.

Because of the limited resolution, this study could not clarify the properties in the very small- $|\omega|$ regime, such as the nature of the excitation in the small- $|\omega|$ limit, the accurate gapless points of the single-particle spectrum, and the presence or absence of a long-range order in the ground state, although a superconducting ground state has been suggested in a considerable number of studies for the 2D t - J model.^{13-16,106-110} Further studies are needed to clarify more details and how the anomalous features are related to high- T_c superconductivity.

Acknowledgments

This work was supported by KAKENHI (Grants No. 23540428 and No. 26400372) and the World Premier International Research Center Initiative (WPI), MEXT, Japan. The numerical calculations were partly performed on the supercomputer at the National Institute for Materials Science.

¹ J. G. Bednorz and K. A. Müller, *Z. Phys. B* **64**, 189 (1986).

² A. Damascelli, Z. Hussain, and Z.-X. Shen, *Rev. Mod. Phys.* **75**, 473 (2003).

³ H. Romberg, M. Alexander, N. Nücker, P. Adelmann, and J. Fink, *Phys. Rev. B* **42**, 8768 (1990).

⁴ C. T. Chen, F. Sette, Y. Ma, M. S. Hybertsen, E. B. Stechel, W. M. C. Foulkes, M. Schluter, S.-W. Cheong, A. S. Cooper, L. W. Rupp, Jr., B. Batlogg, Y. L. Soo, Z. H. Ming, A. Krol, and Y. H. Kao, *Phys. Rev. Lett.* **66**, 104 (1991).

⁵ D. S. Dessau, Z.-X. Shen, D. M. King, D. S. Marshall, L. W. Lombardo, P. H. Dickinson, A. G. Loeser, J. DiCarlo, C.-H. Park, A. Kapitulnik, and W. E. Spicer, *Phys. Rev. Lett.* **71**, 2781 (1993).

⁶ T. Yoshida, X. J. Zhou, K. Tanaka, W. L. Yang, Z. Hussain, Z.-X. Shen, A. Fujimori, S. Sahrakorpi, M. Lindroos, R. S. Markiewicz, A. Bansil, S. Komiya, Y. Ando, H. Eisaki, T. Kakeshita, and S. Uchida, *Phys. Rev. B* **74**, 224510 (2006).

⁷ J. Graf, G.-H. Gweon, K. McElroy, S. Y. Zhou, C. Jozwiak, E. Rotenberg, A. Bill, T. Sasagawa, H. Eisaki, S. Uchida, H. Takagi, D.-H. Lee, and A. Lanzara, *Phys. Rev. Lett.* **98**, 067004 (2007).

⁸ B. P. Xie, K. Yang, D. W. Shen, J. F. Zhao, H. W. Ou, J. Wei, S. Y. Gu, M. Arita, S. Qiao, H. Namatame, M. Taniguchi, N. Kaneko, H. Eisaki, K. D. Tsuei, C. M. Cheng, I. Vobornik, J. Fujii, G. Rossi, Z. Q. Yang, and D. L. Feng, *Phys. Rev. Lett.* **98**, 147001, (2007).

⁹ T. Valla, T. E. Kidd, W.-G. Yin, G. D. Gu, P. D. Johnson, Z.-H. Pan, and A. V. Fedorov, *Phys. Rev. Lett.* **98**, 167003 (2007).

¹⁰ Z.-H. Pan, P. Richard, A. V. Fedorov, T. Kondo, T. Takeuchi, S. L. Li, P. Dai, G. D. Gu, W. Ku, Z. Wang, and H. Ding, arXiv:cond-mat/0610442.

¹¹ B. Moritz, F. Schmitt, W. Meevasana, S. Johnston, E. M. Motoyama, M. Greven, D. H. Lu, C. Kim, R. T. Scalettar, Z.-X. Shen, and T. P. Devereaux, *New J. Phys.* **11**, 093020 (2009).

¹² M. Imada, A. Fujimori, and Y. Tokura, *Rev. Mod. Phys.* **70**, 1039 (1998).

¹³ E. Dagotto, *Rev. Mod. Phys.* **66**, 763 (1994).

¹⁴ P. W. Anderson, *Science* **235**, 1196 (1987).

¹⁵ P. A. Lee, N. Nagaosa, and X.-G. Wen, *Rev. Mod. Phys.* **78**, 17 (2006).

¹⁶ M. Ogata and H. Fukuyama, *Rep. Prog. Phys.* **71**, 036501 (2008).

¹⁷ Y. Yanase, T. Jujo, T. Nomura, H. Ikeda, T. Hotta, and

- K. Yamada, Phys. Rep. **387**, 1 (2003).
- ¹⁸ F. C. Zhang and T. M. Rice, Phys. Rev. B **37**, 3759 (1988).
- ¹⁹ A. B. Harris and R. V. Lange, Phys. Rev. **157**, 295 (1967).
- ²⁰ P. Phillips, T.-P. Choy, and R. G. Leigh, Rep. Prog. Phys. **72**, 036501 (2009).
- ²¹ P. Phillips, Rev. Mod. Phys. **82**, 1719 (2010).
- ²² Y. Yamaji and M. Imada, Phys. Rev. Lett. **106**, 016404 (2011).
- ²³ Y. Yamaji and M. Imada, Phys. Rev. B **83**, 214522 (2011).
- ²⁴ S. Sakai, Y. Motome, and M. Imada, Phys. Rev. Lett. **102**, 056404 (2009).
- ²⁵ D. Sénéchal, D. Perez, and M. Pioro-Ladrière, Phys. Rev. Lett. **84**, 522 (2000).
- ²⁶ D. Sénéchal, D. Perez, and D. Plouffe, Phys. Rev. B **66**, 075129 (2002).
- ²⁷ Y. Nagaoka, Phys. Rev. **147**, 392 (1966).
- ²⁸ X. Y. Zhang, E. Abrahams, and G. Kotliar, Phys. Rev. Lett. **66**, 1236 (1991).
- ²⁹ W. O. Putikka, M. U. Luchini, and M. Ogata, Phys. Rev. Lett. **69**, 2288 (1992).
- ³⁰ V. J. Emery, S. A. Kivelson, and H. Q. Lin, Phys. Rev. Lett. **64**, 475 (1990).
- ³¹ W. O. Putikka, M. U. Luchini, and T. M. Rice, Phys. Rev. Lett. **68**, 538 (1992).
- ³² E. Dagotto, A. Moreo, F. Ortolani, D. Poilblanc, and J. Riera, Phys. Rev. B **45**, 10741 (1992).
- ³³ E. Dagotto, J. Riera, Y. C. Chen, A. Moreo, A. Nazarenko, F. Alcaraz, and F. Ortolani, Phys. Rev. B **49**, 3548 (1994).
- ³⁴ M. Kohno, Phys. Rev. B **55**, 1435 (1997).
- ³⁵ C. S. Hellberg and E. Manousakis, Phys. Rev. Lett. **78**, 4609 (1997).
- ³⁶ C. T. Shih, Y. C. Chen, and T. K. Lee, Phys. Rev. B **57**, 627 (1998).
- ³⁷ M. Calandra, F. Becca, and S. Sorella, Phys. Rev. Lett. **81**, 5185 (1998).
- ³⁸ S. R. White and D. J. Scalapino, Phys. Rev. B **61**, 6320 (2000).
- ³⁹ R. R. P. Singh and D. A. Huse, Phys. Rev. B **40**, 7247 (1989).
- ⁴⁰ M. Kohno, Phys. Rev. Lett. **108**, 076401 (2012).
- ⁴¹ M. G. Zacher, R. Eder, E. Arrigoni, and W. Hanke, Phys. Rev. Lett. **85**, 2585 (2000).
- ⁴² M. Kohno, Phys. Rev. B **90**, 035111 (2014).
- ⁴³ Y. Wang, K. Wohlfeld, B. Moritz, C. J. Jia, M. van Veenendaal, K. Wu, C.-C. Chen, and T. P. Devereaux, arXiv:1505.08143.
- ⁴⁴ E. Jeckelmann, Phys. Rev. B **66**, 045114 (2002).
- ⁴⁵ I. P. McCulloch, A. R. Bishop, and M. Gulacsi, Phil. Mag. B **81**, 1603 (2001).
- ⁴⁶ I. P. McCulloch, Ph.D. thesis, Australian National University (2001).
- ⁴⁷ M. Kohno, arXiv:1507.04828.
- ⁴⁸ X. G. Wen, Phys. Rev. B **42**, 6623 (1990).
- ⁴⁹ M. Kohno, Phys. Rev. Lett. **105**, 106402 (2010).
- ⁵⁰ H. Benthien, F. Gebhard, and E. Jeckelmann, Phys. Rev. Lett. **92**, 256401 (2004).
- ⁵¹ F. H. L. Essler, H. Frahm, F. Göhmann, A. Klümper, and V. E. Korepin, *The One-Dimensional Hubbard Model* (Cambridge University Press, Cambridge, England, 2005).
- ⁵² H. J. Schulz, in *Correlated Electron Systems*, edited by V. J. Emery (World Scientific, Singapore, 1993), p. 199.
- ⁵³ P. A. Bares and G. Blatter, Phys. Rev. Lett. **64**, 2567 (1990).
- ⁵⁴ K. Penc, K. Hallberg, F. Mila, and H. Shiba, Phys. Rev. Lett. **77**, 1390 (1996).
- ⁵⁵ J. Favand, S. Haas, K. Penc, F. Mila, and E. Dagotto, Phys. Rev. B **55**, 4859 (1997).
- ⁵⁶ C. Lavalle, M. Arikawa, S. Capponi, F. F. Assaad, and A. Muramatsu, Phys. Rev. Lett. **90**, 216401 (2003).
- ⁵⁷ R. Eder and Y. Ohta, Phys. Rev. B **56**, 2542 (1997).
- ⁵⁸ M. Kohno, O. A. Starykh, and L. Balents, Nat. Phys. **3**, 790 (2007).
- ⁵⁹ M. Kohno, Phys. Rev. Lett. **103**, 197203 (2009).
- ⁶⁰ H. Eskes, M. B. J. Meinders, and G. A. Sawatzky, Phys. Rev. Lett. **67**, 1035 (1991).
- ⁶¹ E. Dagotto, A. Moreo, F. Ortolani, J. Riera, and D. J. Scalapino, Phys. Rev. Lett. **67**, 1918 (1991).
- ⁶² M. Kohno, JPS Conf. Proc. **3**, 013020 (2014).
- ⁶³ N. Bulut, D. J. Scalapino, and S. R. White, Phys. Rev. B **50**, 7215 (1994).
- ⁶⁴ R. Preuss, W. Hanke, and W. von der Linden, Phys. Rev. Lett. **75**, 1344 (1995).
- ⁶⁵ R. Preuss, W. Hanke, C. Gröber, and H. G. Evertz, Phys. Rev. Lett. **79**, 1122 (1997).
- ⁶⁶ A. Moreo, S. Haas, A. W. Sandvik, and E. Dagotto, Phys. Rev. B **51**, 12045 (1995).
- ⁶⁷ J. Jaklič and P. Prelovšek, Phys. Rev. B **55**, 7307 (1997).
- ⁶⁸ J. Jaklič and P. Prelovšek, Adv. Phys. **49**, 1 (2000).
- ⁶⁹ R. Eder and Y. Ohta, Phys. Rev. B **54**, 3576 (1996).
- ⁷⁰ R. Eder, K. Seki, and Y. Ohta, Phys. Rev. B **83**, 205137 (2011).
- ⁷¹ T. Tohyama, Phys. Rev. B **70**, 174517 (2004).
- ⁷² M. M. Zemljič, P. Prelovšek, and T. Tohyama, Phys. Rev. Lett. **100**, 036402 (2008).
- ⁷³ S. Sakai, Y. Motome, and M. Imada, Phys. Rev. B **82**, 134505 (2010).
- ⁷⁴ Y. Ohta, K. Tsutsui, W. Koshibae, T. Shimozato, and S. Maekawa, Phys. Rev. B **46**, 14022 (1992).
- ⁷⁵ W. Stephan and P. Horsch, Phys. Rev. Lett. **66**, 2258 (1991).
- ⁷⁶ R. Eder, Y. Ohta, and T. Shimozato, Phys. Rev. B **50**, 3350 (1994).
- ⁷⁷ H.-Q. Ding, Physica C **203**, 91 (1992).
- ⁷⁸ R. R. P. Singh and R. L. Glenister, Phys. Rev. B **46**, 14313 (1992).
- ⁷⁹ R. Eder and Y. Ohta, Phys. Rev. B **51**, 6041 (1995).
- ⁸⁰ S. Haas, Phys. Rev. B **51**, 11748 (1995).
- ⁸¹ A. L. Chernyshev, P. W. Leung, and R. J. Gooding, Phys. Rev. B **58**, 13594 (1998).
- ⁸² W. O. Putikka, M. U. Luchini, and R. R. P. Singh, J. Phys. Chem. Solids **59**, 1858 (1998).
- ⁸³ P. W. Leung, Phys. Rev. B **73**, 014502 (2006).
- ⁸⁴ D. Poilblanc, T. Ziman, H. J. Schulz, and E. Dagotto, Phys. Rev. B **47**, 14267 (1993).
- ⁸⁵ E. Dagotto, A. Moreo, R. Joynt, S. Bacci, and E. Gagliano, Phys. Rev. B **41**, 2585 (1990).
- ⁸⁶ E. Dagotto, R. Joynt, A. Moreo, S. Bacci, and E. Gagliano, Phys. Rev. B **41**, 9049 (1990).
- ⁸⁷ S. Schmitt-Rink, C. M. Varma, and A. E. Ruckenstein, Phys. Rev. Lett. **60**, 2793 (1988).
- ⁸⁸ S. A. Trugman, Phys. Rev. B **37**, 1597 (1988).
- ⁸⁹ C. L. Kane, P. A. Lee, and N. Read, Phys. Rev. B **39**, 6880 (1989).
- ⁹⁰ S. Sachdev, Phys. Rev. B **39**, 12232 (1989).
- ⁹¹ C. J. Hamer, Z. Weihong, and J. Oitmaa, Phys. Rev. B

- 58**, 15508 (1998).
- ⁹² K. J. von Szczepanski, P. Horsch, W. Stephan, and M. Ziegler, *Phys. Rev. B* **41**, 2017 (1990).
- ⁹³ F. Marsiglio, A. E. Ruckenstein, S. Schmitt-Rink, and C. M. Varma, *Phys. Rev. B* **43**, 10882 (1991).
- ⁹⁴ G. Martínez and P. Horsch, *Phys. Rev. B* **44**, 317 (1991).
- ⁹⁵ Z. Liu and E. Manousakis, *Phys. Rev. B* **45**, 2425 (1992).
- ⁹⁶ P. Béran, D. Poilblanc, and R. B. Laughlin, *Nucl. Phys. B* **473**, 707 (1996).
- ⁹⁷ M. Brunner, F. F. Assaad, and A. Muramatsu, *Phys. Rev. B* **62**, 15480 (2000).
- ⁹⁸ É. L. Nagaev, *Sov. Phys. JETP* **31**, 682 (1970).
- ⁹⁹ A. Macridin, M. Jarrell, T. Maier, and D. J. Scalapino, *Phys. Rev. Lett.* **99**, 237001 (2007).
- ¹⁰⁰ F. Tan, Y. Wan, and Q.-H. Wang, *Phys. Rev. B* **76**, 054505 (2007).
- ¹⁰¹ C. Weber, K. Haule, and G. Kotliar, *Phys. Rev. B* **78**, 134519 (2008).
- ¹⁰² E. Dagotto, A. Nazarenko, and M. Boninsegni, *Phys. Rev. Lett.* **73**, 728 (1994).
- ¹⁰³ H. Eskes and R. Eder, *Phys. Rev. B* **54**, 14226 (1996).
- ¹⁰⁴ M. Takahashi, *Thermodynamics of One-Dimensional Solvable Models* (Cambridge University Press, Cambridge, England, 1999).
- ¹⁰⁵ P. W. Anderson, *Phys. Rev.* **86**, 694 (1952).
- ¹⁰⁶ E. Dagotto and J. Riera, *Phys. Rev. Lett.* **70**, 682 (1993).
- ¹⁰⁷ J. A. Riera and A. P. Young, *Phys. Rev. B* **39**, 9697 (1989).
- ¹⁰⁸ C. Gros, *Phys. Rev. B* **38**, 931 (1988).
- ¹⁰⁹ H. Yokoyama and H. Shiba, *J. Phys. Soc. Jpn.* **57**, 2482 (1988).
- ¹¹⁰ S. Sorella, G. B. Martins, F. Becca, C. Gazza, L. Capriotti, A. Parola, and E. Dagotto, *Phys. Rev. Lett.* **88**, 117002 (2002).